Tetrahedrally Coordinated Iron(II) Incorporation in the Super-Sodalite Aluminophosphate $Fe_3Al_6(PO_4)_{12}{\cdot}4tren{\cdot}17H_2O$ (MIL-74)

Lionel Beitone,[†] Thierry Loiseau,*[,†] Franck Millange,[†] Clarisse Huguenard,[§] Gerhard Fink,[§] Francis Taulelle,[§] Jean-Marc Grenèche,[||] and Gérard Férey[†,‡]

Institut Lavoisier (UMR CNRS 8637) and Institut Universitaire de France, Université de Versailles St Quentin en Yvelines, 45 Avenue des Etats Unis, 78035 Versailles, France, Tectonique Moléculaire du Solide UMR 7140, Université Louis Pasteur, 4 rue Blaise Pascal, 67000 Strasbourg France, and Laboratoire de Physique de l'Etat Condensé, UMR CNRS 6087, Université du Maine, Avenue O. Messiaen, 72085 Le Mans Cedex 9, France

Received June 25, 2003. Revised Manuscript Received September 10, 2003

An iron−aluminum phosphate $Fe_3Al_6(PO_4)_{12}{\cdot}4tren{\cdot}17H_2O$ (MIL-74) has been hydrothermally synthesized with the tris(2-aminoethyl)amine (*tren*) as a structure-directing agent (453 K, 36 h, autogenous pressure). Single-crystal X-ray diffraction, magnetic measurements, and Mössbauer and solid-state NMR spectroscopies were carried out to characterize the compound. Its crystal structure is cubic, $a = 16.7705(1)$ Å and may be described as $I\bar{4}3m$ or $P\bar{4}3n$ depending on the degree of cationic ordering. The open framework is built up from an enneameric unit (T = Fe, Al) containing five TO_4 and four PO_4 tetrahedra (one of the P−O bonds is terminal). A central AlO_4 tetrahedral unit shares all its corners with four phosphates groups. Two phosphate groups are connected to two other peripheral TO_4 units. This results in the formation of a "pseudo" planar building block T_5P_4 consisting of four square 4-rings. The connection of the T_5P_4 units generates a three-dimensional framework, which defines a super-sodalite topology. The resulting cavities (diameter of 10 Å) are bound by 12-ring windows in which are located the *tren* species in interaction with the phosphate groups (mainly terminal P−O bonding) through hydrogen bonds. A cluster of 17 water molecules occupies the center of the super-sodalite cage. The Mössbauer spectroscopy shows that divalent iron cations are incorporated into the framework with an unusual tetrahedral coordination. Despite the existence of the paramagnetic cations Fe^{2+} in the inorganic network, ^{31}P, ^{27}Al, and ^{1}H solid state NMR signatures could be obtained with a relatively significant resolution. The spectroscopic methods indicate a certain degree of cationic ordering between Al and Fe occurs on the peripheral T sites of the enneameric building unit (correlated to a lower symmetry, $P\bar{4}3n$), although the X-ray diffraction analysis shows a disordering situation (space group $I\bar{4}3m$).

Introduction

Nanoporous materials with their wide variety of three-dimensional topologies are very flexible materials. They potentially offer many applications[1−3] in different domains such as catalysis, ionic exchangers, gas separation, and purification, because they can integrate many different chemical elements. Historically, only the zeolites-type aluminosilicates family was concerned, but the phosphates-based compounds have received considerable attention since the nanoporous aluminum phosphates preparation reported by researchers of Union Carbide Corporation[4] in early 1980s. This breakthrough opened up new investigations, and during the last two decades other chemical elements such as gallium, indium, germanium, or transition metals (3d), were used for the production of a large variety of inorganic open-framework solids.[5,6] The compounds are typically synthesized under mild hydrothermal conditions in the presence of organic molecules (amines, quaternary tetralkylammonium salts, etc.), which direct the formation of a porous system and enhance the structural diversity of three-dimensional architectures.

Besides the interest of new structures, special attention has been paid to chemical modification of the inorganic network to improve the chemical reactivity. For instance, despite their structural similarity to zeolites (tetrahedral units TO_4 connection), the alumi-

* To whom correspondence should be addressed. Phone: 33 1 39 254 373. Fax: 33 1 39 254 358. E-mail: loiseau@chimie.uvsq.fr.
† Institut Lavoisier, Université de Versailles St Quentin en Yvelines.
‡ Institut Universitaire de France, Université de Versailles St Quentin en Yvelines.
§ Université Louis Pasteur.
|| Université du Maine.

(1) Davis, M. E. *Nature*, **2002**, *417*, 813.
(2) Davis, M. E.; Lobo, R. F. *Chem. Mater.* **1992**, *4*, 756.
(3) Corma, A. *Chem. Rev.* **1995**, *95*, 559.
(4) Wilson, S. T.; Lok, B. M.; Messina, C. A.; Cannan, T. R.; Flanigen, E. M. *J. Am. Chem. Soc.* **1982**, *104*, 1146.
(5) Cheetham, A. K.; Férey, G.; Loiseau T. *Angew. Chem., Int. Ed. Engl.* **1999**, *38*, 3268.
(6) Baerlocher, C.; Meier, W. M.; Olson, D. H. *Atlas of Zeolite Framework Types*, 5th rev. ed.; Elsevier Science B. V.: Amsterdam, The Netherlands, 2001.

10.1021/cm034535d CCC: $25.00
Published on Web 10/22/2003

Table 1. Reactant Gel Molar Compositions for the Synthesis of $Fe_3Al_6(PO_4)_{12}$·4*tren*·$17H_2O$ (MIL-74)

no.	iron precursor	$Al(OH)_3$	H_3PO_4	H_2O	tren	product
1	iron metal (Fe, 99%, RDH), 0.5 Fe (0.10 g)	1 $Al(OH)_3$ (0.27 g)	2 H_3PO_4 (0.80 g)	80 H_2O (4.85 g)	1.7 *tren* (0.86 g)	colorless crystals
2	iron(II) chloride ($FeCl_2$·$4H_2O$, 99%, Merck), 0.5 $FeCl_2$ (0.34 g)	1 $Al(OH)_3$ (0.27 g)	2 H_3PO_4 (0.80 g)	80 H_2O (4.85 g)	1.9 *tren* (0.96 g)	brown crystal
3	iron(III) chloride ($FeCl_3$·$6H_2O$, 99+%, Alfa), 0.5 $FeCl_3$ (0.47 g)	1 $Al(OH)_3$ (0.27 g)	2 H_3PO_4 (0.80 g)	80 H_2O (4.85 g)	2.1 *tren* (1.06 g)	black crystals

num phosphates series exhibits significantly different chemical properties. The porous $AlPO_4$ compounds have a neutral framework, and the partial substitution of aluminum by other metal elements with a different oxidation state (for example, silicon or divalent transition metals) is required for generating hydroxyl groups and Brönsted acidity in this class of materials.[7] The strategy lies in the choice of periodic table elements that may adopt a tetrahedral coordination to be incorporated into the TO_4 tetrahedra-based network.[8] Some 3d transition metals were found to be good candidates, and a large number of works reported the incorporation of Mn^{2+}, Co^{2+}, Ti^{4+}, etc. into the porous $AlPO_4$ materials, which are catalytically active.[9]

In this context, several studies described the iron substitution in different $AlPO_4$-*n* phases and Flanigen and co-workers, with the characterization of compounds called FAPO-*n*,[10] first claimed it. The incorporation of the iron cations was particularly investigated in the $AlPO_4$-5,[11−13] -11,[14−16] -18,[17] and -31[13] phases. Tetrahedrally coordinated iron atoms were usually observed with the oxidation state 3+ in the $AlPO_4$ matrix, and the iron substituted aluminophosphates have shown very efficient chemical activity for some specific catalytic reactions (i.e., cyclohexane oxidation[12,13]).

The crystal chemistry of the iron phosphates is also very rich and the structures of many natural minerals have been described.[18] It includes different types of coordination for the iron atoms (tetrahedron, trigonal bipyramid, and octahedron). Among them, the mixed aluminum−iron phosphate cacoxenite[19] represents the most remarkable example of this family. Its open framework is built up from extra large channels of 14.2 Å, in which water molecules are trapped. More recently, following the strategy initiated by Flanigen for the preparation of the $AlPO_4$-*n* series,[4] new synthetic iron phosphates have been prepared in the presence of organic structure-directing agents.[20,21]

However, the incorporation of divalent iron is rarely reported in the phosphates. The iron(II) cations usually exhibit the 6- (octahedral) and 5-fold (trigonal bipyramid) coordinations (see refs 22−25, for instance). The occurrence of the tetrahedral coordinated iron(II) cations is described in a few examples. They are present in the mixed valence Fe^{3+}/Fe^{2+} FAPO-*n* solids[15,16] and the two organically templated iron phosphates $Fe_4O(PO_4)_4$·2*en*·H_2O[26] (Fe^{2+}/Fe^{3+}) and $FePO_4$·*en*[27] (Fe^{2+}) (*en* is ethylenediamine).

In this paper a mixed iron aluminum phosphate $Fe_3Al_6(PO_4)_{12}$·4*tren*·$17H_2O$ has been prepared. Its structure is similar to that of the zinc−aluminum phosphate MIL-74 (Zn).[28] The phase contains divalent iron cations with a tetrahedral coordination, incorporated into an $AlPO_4$ three-dimensional framework. ^{57}Fe Mössbauer spectroscopy was used to optimize the synthesis and prove the presence of iron(II) excluding iron(III). High-resolution solid state NMR spectroscopy was performed on this paramagnetic compound with relatively well resolved spectra for ^{31}P as well as ^{27}Al.

Experimental Section

Synthesis. The iron−aluminum phosphate $Fe_3Al_6(PO_4)_{12}$·4*tren*·$17H_2O$ (MIL-74) was hydrothermally prepared from a mixture of aluminum hydroxide ($Al(OH)_3$, Aldrich), phosphoric acid (H_3PO_4, 85%, Prolabo), tris(2-aminoethyl)amine ($N_4C_6H_{18}$, 95%, Avocado), deionized water, and a source of iron. Different precursors of iron (iron metal, iron(II) chloride, and iron(III) chloride) could be used for the synthesis of MIL-74. The different molar compositions are reported in Table 1. The reactants were magnetically stirred during 5 min, sealed into a 23-mL Teflon-lined Parr bomb, and heated at 453 K for 36 h under autogenous pressure before cooling during 12 h down to room temperature. The initial and final pH values were both ca. 9−10. The powdered samples were collected by filtration,

(7) Lok, B. M.; Messina, C. A.; Patton, R. L.; Gajek, R. T.; Cannan, T. R.; Flanigen, E. M. *J. Am. Chem. Soc.* **1984**, *106*, 6092.
(8) Flanigen, E. M.; Lok, B. M.; Patton, R. L.; Wilson, S. T. *Pure Appl. Chem.* **1986**, *58*, 1351.
(9) Thomas, J. M. *Angew. Chem., Int. Ed. Engl.* **1999**, *38*, 3588.
(10) Messina, C. A.; Lok; B. M.; Flanigen, E. M. Eur. Pat. 131,946, 1984.
(11) Cardile, C. M.; Tapp, N. J.; Milestone, N. B. *Zeolites* **1990**, *10*, 90.
(12) Raja, R.; Sankar, G.; Thomas, J. M. *J. Am. Chem. Soc.* **1999**, *121*, 11926.
(13) Dugal, M.; Sankar, G.; Raja, R.; Thomas, J. M. *Angew. Chem., Int. Ed.* **2000**, *39*, 2310.
(14) Dai, P.-S.; Petty, R. H.; Ingram, C. W.; Szostak, R. *Appl. Catal. A.* **1996**, *143*, 101.
(15) Lázár, K.; Žilková, N.; Čejka, J. In *Zeolites and Mesoporous Materials at the Dawn of the 21st Century*; Galarneau, A., Di Renzo, F., Fajula, F., Vedrine, J., Eds.; Vol. 135 in Studies in Surface Science and Catalysis Series; Elsevier: New York, 2001; pp 14−22.
(16) Lázár, K.; Chandwadkar, A. J.; Fejes, P.; Čejka, J.; Ramaswamy, A. V. *J. Radioanal. Nucl. Chem.* **2000**, *246*, 143.
(17) Zenonos, C.; Beale, A.; Sankar, G.; Lewis, D.; Thomas, J. M.; Catlow, R. A. In *Zeolites and Mesoporous Materials at the Dawn of the 21st Century*; Galarneau, A., Di Renzo, F., Fajula, F., Vedrine, J., Eds.; Vol. 135 in Studies in Surface Science and Catalysis Series; Elsevier: New York, 2001; pp 14−39.
(18) Moore, P. B. *Am. Mineral.* **1970**, *55*, 135.
(19) Moore, P. B.; Shan, J. *Nature* **1983**, *306*, 356.
(20) Lii, K.-H.; Huang, Y.-F.; Zima, V.; Huang, C.-Y.; Lin, H.-M.; Jiang, Y.-C.; Liao, F.-L.; Wang, S.-L. *Chem. Mater.* **1998**, *10*, 2599.
(21) Riou-Cavellec, M.; Riou, D.; Férey, G. *Inorg. Chim. Acta* **1999**, *291*, 317.
(22) Kostiner, E.; Rea, J. R. *Inorg. Chem.* **1974**, *13*, 2876.
(23) Moore, P. B.; Araki, T. *Am. Mineral.* **1975**, *60*, 454.
(24) Bouchdoug, M.; Courtois, A.; Gerardin, R.; Steinmetz, J.; Gleitzer, C. *J. Solid State Chem.* **1982**, *42*, 149.
(25) Guse, W.; Klaska, K. H.; Saalfeld, H.; Adiwidjaja, G. *Neues Jahrb. Mineral. Monatsh.* **1985**, *10*, 433.
(26) De Bord, J. R. D.; Reiff, W. M.; Warren, C. J.; Haushalter, R. C.; Zubieta, J. *Chem. Mater.* **1997**, *9*, 1994.
(27) Na, L.-Y.; Liu, Y.-L.; Pang, W.-Q.; Xu, R.-R. *Chinese J. Inorg. Chem.* **2000**, *16*, 287.
(28) Beitone, L.; Huguenard, C.; Gansmuller, A.; Henry, M.; Taulelle, F.; Loiseau, T.; Férey, G. *J. Am. Chem. Soc.* **2003**, *125*, 9102.

washed with purified water, and dried at room temperature. The purity of the products was checked by powder X-ray diffraction. Depending on the oxidation state of the iron source, the MIL-74 solid crystallizes with different colors: it is colorless with iron metal, brown with iron(II) chloride, or black with iron(III) chloride. The color is directly correlated to the variation of the amount (0−6%) of Fe^{3+} incorporated into the FeAlPO matrix (see ^{57}Fe Mössbauer study section). The optical microscope examination shows that the MIL-74 compound is obtained with a specific well-defined crystal morphology corresponding to a rhombododecahedron shape (consisting of twelve rhombic faces). The particle size observed by scanning electron microscope is in the range 50−400 μm. This crystal-shape feature was previously reported for the zinc−aluminum phosphate[28] analogous solid.

Elemental Analysis. Fe, Al, P, C, N, and H chemical analyses were performed by ICP emission spectroscopy at the National Center of Analysis of CNRS (Vernaison, France). The elemental analysis of the sample gave the following results according to the chemical formula of the title compound $Fe_3Al_6(PO_4)_{12}$·4*tren*·$17H_2O$ (weight %): Fe, 7.8 (calc. 7.1); Al, 6.8 (calc. 6.2); P, 16.3 (calc. 15.7); C, 12.1 (calc. 12.1); N, 9.4 (calc. 9.4); H, 4.8 (calc. 5.0).

Thermal Analysis. TGA measurements were obtained using a TGA 2500 thermogravimetric analyzer (TA Instruments) with a heating rate of 2 K·mn^{-1} under O_2 atmosphere up to 1073 K. Upon heating, the thermogravimetric analysis revealed a continuous weight loss from room temperature to 1023 K, and its interpretation was quite delicate. Nevertheless, two distinct events were observed. Before 553 K, a first weight loss could be assigned to the departure of water molecules encapsulated in the structure cavities (obs, 13.8%; calc, 12.9%). A second event would then be attributed to the removal of the amine species of the compound (obs, 26.2%; calc, 25.2%). At 1073 K, the powder X-ray diffraction analysis of the black residue indicated that the structure of the titled solid was collapsed and it was transformed into a mixture of a dense aluminophosphate ($AlPO_4$ cristobalite type, JCPDS file 11-0500) and an amorphous phase.

Single-Crystal X-ray Diffraction. A suitable crystal was carefully selected and glued onto a glass fiber. The X-ray data were recorded at room temperature on a Bruker SMART three-circle diffractometer with a CCD bidimensional detector (monochromatized Mo Kα radiation). The crystal-to-detector distance was 45 mm allowing for the data collection up to 60° (2θ). Slightly more than one hemisphere of data was recorded. Crystal data and details of the data collection are given for the space group $I\bar{4}3m$ (n*o*. 217) in Table 2. An empirical absorption correction was applied using the SADABS[29] program based on the method of Blessing.[30] The structure was refined by full-matrix least squares using the SHELX-TL package.[31] The atomic positions of the parent zinc−aluminum phosphate MIL-74[28] structure were used for a starting model in the space group $I\bar{4}3m$. The partial occupancy of aluminum by iron atoms on the site 12*d* was not considered in a first step. A full occupancy of the aluminum or iron on the site 12*d* led to the reliability factors R1 = 0.1876 and R1 = 0.0592, respectively. In both cases, the thermal parameters of the corresponding atoms converge to zero. Then the occupancy factor of the site 12*d* was refined and converges to a ratio close to 57(1):43(1) for Al/Fe with R1 = 0.0320. A similar calculation was carried out for the site 6*b* but the factor converges to occupancy greater than 97% for aluminum and this site was considered as fully occupied by aluminum. Finally, the occupancy factor was fixed to 50% for the occupancy of Al/Fe on site 12*d* in order to be in agreement with the chemical analysis (Al/Fe ratio of 2) and the electroneutrality of the structure. One of two inequivalent crystallographically carbon atom sites (labeled C(1)) is split on two positions and has an occupancy factor of 50%. Hydrogen atoms of amine and water molecules were not placed, and anisotropic displacement parameters of all atoms (except those of Al(2) or Fe(2) on site 12*d*; their displacement parameters were refined isotropically and were found to be equal) were considered in the final refinement. The corresponding reliability factors converge to R1 = 0.0327 and wR2 = 0.0991 (for 1245 reflections $I > 2\sigma(I)$ and 66 parameters) in the correct enantiomer. As suggested in our previous work concerning the structure determination of zinc aluminum phosphate MIL-74,[28] the structure was also refined in space group $P\bar{4}3n$ (n*o*. 218). In the latter case, the site 12*d* is split into two crystallographic positions 6*c* and 6*d*, and the Al/Fe occupancy factors refine to 49(1)/51(1) for 6*c* and 56(1)/44(1) for 6*d* with R1 = 0.0563. XRD does not show a strict Fe/Al order occurring on the tetrahedral sites of the structure. A similar observation was reported in the aluminum phosphate analogue incorporating zinc.[28] Table 3 provides the final atomic positions and isotropic thermal parameters.

Table 2. Crystal Data and Structure Refinement for MIL-74 ($Fe_3Al_6(PO_4)_{12}$·4*tren*·$17H_2O$)

identification code	MIL-74
empirical formula	$Fe_3Al_6P_{12}O_{65}N_{16}C_{24}H_{118}$
formula weight	2372.41 g/mol
temperature	293(2) K
wavelength	0.71073 Å
crystal system, space group	cubic, $I\bar{4}3m$
unit cell dimensions	a = 16.7705(1) Å
volume	4716.70(5) Å^3
Z, calculated density	2, 1.670 mg/m^3
absorption coefficient	0.829 mm^{-1}
F(000)	2460
crystal size	0.36 × 0.36 × 0.36 mm
theta range for data collection	2.43−29.80 deg.
limiting indices	$-22 <= h <= 23$, $-23 <= k <= 23$, $-23 <= l <= 8$
reflections collected/unique	16616/1245 [R(int) = 0.0183]
completeness to theta = 29.80	97.7%
refinement method	full-matrix least-squares on F^2
data/parameters	1245/66
goodness-of-fit on F^2	1.250
final R indices [$I > 2\sigma(I)$]	R1 = 0.0327[a], wR2 = 0.0991[b]
R indices (all data)	R1 = 0.0328[a], wR2 = 0.0993[b]
absolute structure parameter	0.05(4)
extinction coefficient	0.0009(5)
largest diff. peak and hole	0.635 and −0.434 e·Å^{-3}

[a] $R1 = \Sigma||F_o| - |F_c||/\Sigma|F_o|$. [b] $wR2 = \{\Sigma[w(|F_o|^2 - |F_c|^2)^2]/\Sigma[w(|F_o|^2)^2]\}^{1/2}$, $w = 1/[\sigma^2(F_o^2)+(0.00640P)^2 + 2.34P]$ where $P = [(F_o^2)+2F_c^2]/3$

Table 3. Atomic Coordinates (×10^4) and Equivalent Isotropic Displacement Parameters (Å^2 × 10^3) for MIL-74 ($Fe_3Al_6(PO_4)_{12}$·4*tren* ·$17H_2O$) in $I\bar{4}3m$

	x	*y*	*z*	*U*(eq)[a]
Al(1)	10000	5000	5000	17(1)
Al(2)[b]	10000	5000	7500	18(1)
Fe(2)[b]	10000	5000	7500	18(1)
P	9333(1)	3769(1)	6231(1)	21(1)
O(1)	8482(1)	3568(1)	6432(1)	40(1)
O(2)	9800(1)	4066(1)	6963(1)	39(1)
O(3)	9362(1)	4419(1)	5581(1)	33(1)
N(1)	8009(2)	1991(2)	8009(2)	25(1)
C(1)[b]	7563(3)	1777(3)	8732(3)	34(1)
C(2)	11733(2)	3571(1)	6429(1)	36(1)
N(2)	8044(1)	3741(2)	8044(1)	34(1)
O(1W)	5000	5000	5000	138(9)
O(2W)	4066(5)	4066(5)	4066(5)	119(4)
O(3W)	7394(5)	4462(5)	5538(5)	297(10)

[a] *U*(eq) is defined as one-third of the trace of the orthogonalized Uij tensor. [b] Occupancy factor fixed at 50%.

^{57}Fe Mössbauer Spectrometry. Mössbauer experiments were performed at 300, 77, and 4.2 K by means of a bath cryostat, using a constant acceleration spectrometer and a cobalt source diffused into a rhodium matrix. The values of the isomer shift are quoted relative to that of α−Fe foil at 300 K. The hyperfine parameters were refined using a least-

(29) Sheldrick, G. M. SADABS, a program for the Siemens Area Detector ABSorption correction; University of Göttingen, 1995.
(30) Blessing, R. *Acta Crystallogr*. **1995**, *A51*, 33.
(31) Sheldrick, G. M. SHELXTL version 5.03, software package for the Crystal Structure Determination; University of Göttingen, 1994.

squares fitting procedure in the MOSFIT program.[32]

Magnetic Study. Magnetic susceptibility measurement was made with a superconducting quantum interference device (SQUID) magnetometer (MPMS quantum design) in the temperature range 5−300 K. This dc susceptibility measurement was carried out at low field (10 mT) with increasing temperature after the sample was zero-field cooled. Field dependence magnetization of MIL-74 was also measured up to 5.5 T at 5 K.

NMR Spectroscopy. NMR spectra of ^{31}P and ^{27}Al have been acquired on a DSX 500 spectrometer from Bruker at a field of 11.7 T. A 4-mm MAS probe was used for both ^{31}P and ^{27}Al. Chemical shifts were referenced to their standard chemical shift references, H_3PO_4 85% for ^{31}P and a water solution of $Al(NO_3)_3$ for ^{27}Al. Single pulse excitation was used with the following parameters. Resonating frequencies were 202.416 and 130.295 MHz for ^{31}P and ^{27}Al, respectively. The MAS spinning speed was 10 or 12.5 kHz. Repetition delays were very short for both nuclei, 0.2 s, at contrast with their diamagnetic equivalents. A pulse of 3 μs was used for exciting ^{27}Al for a radio frequency field of 45 kHz. For ^{31}P the pulse length was 2 μs for 62.5 kHz of radio frequency field. Spectral widths were 125 kHz for ^{31}P and 1 MHz for ^{27}Al. The number of acquired points was 4000 for ^{31}P and 16 000 for ^{27}Al.

Results and Discussion

Structure Description. The structure of $Fe_3Al_6(PO_4)_{12}\cdot 4tren\cdot 17H_2O$ (MIL-74) is similar to that of the previously reported zinc−aluminum phosphate[28] (MIL-74). It consists of a strict alternation of PO_4 and TO_4 (T refers to the tetrahedrally coordinated atoms Al^{3+} or Fe^{2+}) tetrahedral polyhedra which are corner sharing. Only iron with an oxidation state of 2+ is incorporated into the framework. The Mössbauer study confirms that point (see section below). Nevertheless, a small amount of Fe^{3+} cations (a few percent) is present when some specific iron precursors are used ($FeCl_2$ or $FeCl_3$) for the synthesis. The asymmetric unit comprises a central AlO_4 species (special position *6b*) connected to four PO_4 groups (special position *24g*). Two adjacent PO_4 units are linked to an additional TO_4 one (special position *12d*) by forming a 4-ring cycle. This results in four adjacent 4-ring units, which form a distorted square enneameric building block T_5P_4 (Figure 1). The T (Al or Fe) atoms are located at the center and the corner of the square unit and lie in a plane, whereas the phosphorus atoms point alternatively above and below the T_5 plane with an up−down−up−down sequence. The P−O distances are in the typical range 1.505(2)−1.543(2) Å for a tetrahedral coordination. One P−O(1) bond (1.505(2) Å) is terminal. The T−O distances differ for both crystallographic positions *6b* and *12d*. For central site *6b*, the Al(1)−O distance is 1.744(2) Å, consistent with that of the tetrahedral surrounding for aluminum. This is in contrast with the situation of peripheral site *12d*, which exhibits a longer T(2)−O distance (1.838(2) Å). This distance lengthening reflects the 50/50 statistical occupancy of aluminum or iron on this specific position. The observed T(2)−O distance of 1.838(2) Å corresponds to the average value of the Al−O bond (1.74 Å) and the expected Fe−O bond for iron(II) in tetrahedral coordination (1.98 Å, calculated from the consideration of the effective ionic radii listed by Shannon and Prewitt[33]). In the choice of the $P\bar{4}3n$ space group, the T(2) site is split into two sites, *6c* and *6d*, and a slight distance contrast is observed for both T−O bonding: they are 1.859(3) Å for site *6c* and 1.808(3) Å for site *6d*. This variation agrees with the Al/Fe distribution difference; the calculated amount of iron is slightly more important on site *6c*.

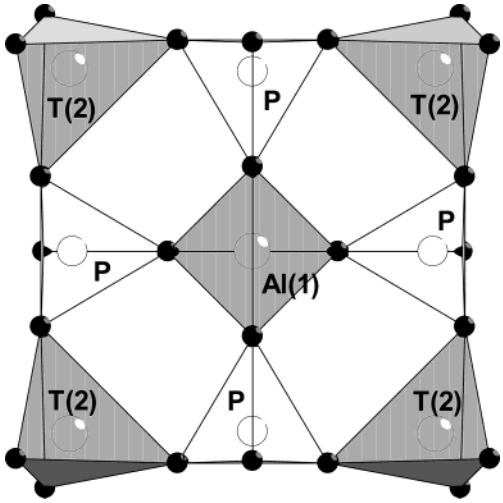

Figure 1. Polyhedral representation of the enneameric building unit T_5P_4 in MIL-74. In the $I\bar{4}3m$ space group, the phosphorus (white tetrahedra) are on the site *24g*, the aluminum Al(1) (gray tetrahedron) is located on the center of the T_5P_4 unit (site *6b*), and the site T(2) (*12d*) is statistically occupied by aluminum or iron (peripheral gray tetrahedra). In the $P\bar{4}3n$ space group, the latter crystallographic position is split into two sites, *6c* and *6d*. Oxygen is represented by black circles.

The T_5P_4 building blocks are connected together through the free T−O bonds of the TO_4 group located at the corner of the square unit, the P−O(1) bond remaining terminal. This connection mode generates a three-dimensional framework related to the sodalite (SOD[6]) arrangement. The square faces of the truncated octahedra of the simple sodalite cage are replaced by faces with four 4-ring units in MIL-74. The topology of MIL-74, which may be called "super sodalite", was previously reported in the aluminum phosphate $Al_9(PO_4)_{12}\cdot C_{24}H_{91}N_{16}\cdot 17H_2O$[34] or the vanadium arsenate $V_8^{4+}V_2^{5+}As_2O_{26}(H_2O)\cdot 8H_2O$.[35] Both structures are described in space group $nI\bar{4}3m$ with a cell parameter of ≈16.7 Å. The sodalite topology is also described in several space groups as a function of the observed cationic ordering (disorder, $nI\bar{4}3m$; order, $P\bar{4}3n$) The resulting "super-sodalite" cavity is bounded by six enneameric units along (100) and eight 12-membered windows (Figure 2) along (111) (instead of hexagonal ones in sodalite structure). However, the free window aperture size is reduced to ≈2.1 Å because of the terminal P−O(1) bonding pointing toward its center. The central nitrogen atoms N(1) of the *tren* molecules also lie on the 3 axis of the structure, at the middle of each 12-membered ring, and the *tren* species fill the window (Figure 3). The terminal nitrogen atoms N(2) of *tren* interact via hydrogen bond with two oxygen atoms O(1) (P−O(1)···N(2) = 2.816(2) Å). The terminal

(32) Teillet, J.; Varret, F. MOSFIT Program, unpublished.
(33) Shannon, R. D.; Prewitt, C. T. *Acta Crystallogr. B* **1969**, *25*, 925.
(34) Xu, Y.-H.; Zhang, B.-G.; Chen, X.-F.; Liu, S.-H.; Duan, C.-Y.; You, X.-Z. *J. Solid State Chem.* **1999**, *145*, 220.
(35) Zhao, Y.; Li, Y.; Liu, Q.; Chen, X.; Wang, Y.; Li, X.; Li, M.; Mai, Z. *J. Solid State Chem.* **2002**, *169*, 160.

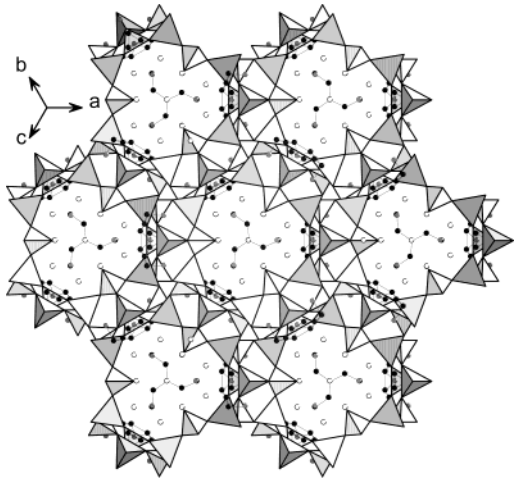

Figure 2. Structure of $Fe_3Al_6(PO_4)_{12}$·4*tren*·$17H_2O$ (MIL-74) along [111] showing the 12-ring windows obstructed by the *tren* molecules.

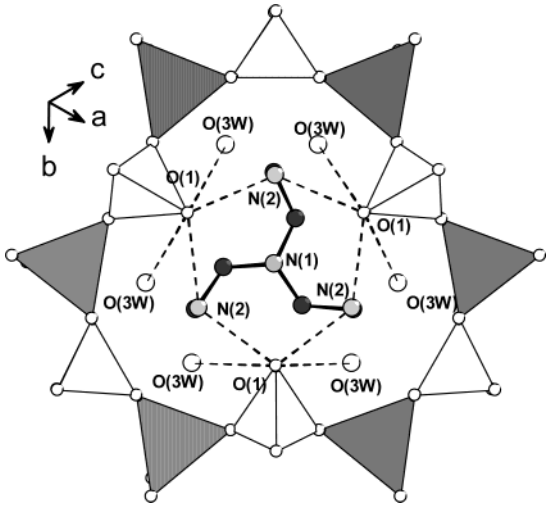

Figure 3. Hydrogen bond interaction scheme of the *tren* molecule with the terminal P−O(1) bond and the water molecules O(3W) in the 12-ring window of MIL-74.

nitrogen atoms N(2) of *tren* species are assumed to be protonated because the central nitrogen N(1) is not. This is based from consideration of the pK_a values which are in the range 9−10 for the terminal nitrogen N(2) and less than 2 for the central one N(1). One carbon (C(1)) of the branched tetramine is disordered on two equivalent positions. The triprotonated organic molecule $[N_4C_6H_{21}]^{3+}$ ensures the electroneutrality of the framework, which has three negative charges $[Fe_3Al_6(PO_4)_{12}]^{3-}$ balanced by the three additional protons of *tren*. The super-sodalite cavity with dimensions of 10 Å (measured between oxygen centers using an ionic radius of 1.35 Å) encapsulates a cluster of 17 water molecules, which exhibits an original atomic packing. The center of the cage is occupied by one water molecule (O(1W) on site *2a*) tetrahedrally linked to four other water molecules O(2W) with O(1W)···O(2W) distances of 2.713(8) Å. O(2W) are then tetrahedrally connected to O(1W) and three other water molecules O(3W) (O3W···O(2W) = 2.62(1) Å). The latter water molecule interacts through hydrogen bond with the terminal oxygen O(1) atom of the phosphate group (O(1)···O(3W) = 2.797(9) Å). The O(iW)···O(jW) hydrogen bonds are shorter than those encountered in the different ice varieties and this

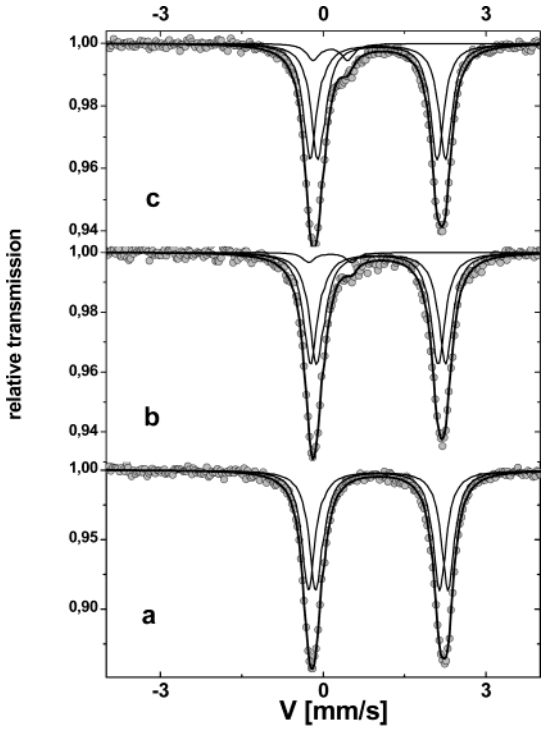

Figure 4. ^{57}Fe Mössbauer spectra recorded at 77 K of the phase $Fe_3Al_6(PO_4)_{12}$·4*tren*·$17H_2O$ (MIL-74) coming from the reaction batch **1** (a) iron metal precursor; **2** (b) iron(II) chloride precursor; **3** (c) iron(III) chloride precursor.

unusual relative high compactness will be detailed in another work.[36]

The occurrence of such a large cavity induces a very low framework density for this three-dimensional architecture. It is 8.9 T per 1000 Å^3 (T = tetrahedral cations) whereas a value of 12.7 is reported in the large pore aluminosilicate faujasite.[6]

^{57}Fe Mössbauer Spectrometry. Mössbauer spectra were recorded at 4.2, 77, and 300 K on three polycrystalline-powdered samples corresponding to the different starting reaction gels **1**, **2**, and **3,** as described in the synthesis section. Some examples of spectra recorded at 77 K are presented in Figure 4: the hyperfine structures result, whatever the temperature is, from a quadrupolar doublet which has to be fitted with at least two components, and, for samples **2** and **3**, a small quadrupolar component which is located at the wing of the low energy line, has to be added. It is important to emphasize that this latter component remains difficult to describe accurately due to both its poor resolution and low content; some constraints were thus considered during the fitting procedure. The refined values of hyperfine parameters of the Mössbauer spectra series obtained at 300, 77, and 4.2 K are listed in Table 4. The main quadrupolar component shows isomer shifts δ of about 1.03(5) mm/s and quadrupolar splitting ΔE in the range of 2.26(5)−2.56(5) mm/s at 300 K. These values are typical of the high spin state Fe^{2+} with a tetrahedral coordination. According to the rather low value of isomer shift, the second component is ascribed to trivalent iron located in tetrahedral sites.

The presence of two components suggests the occurrence of two distinct crystallographic sites for iron in

(36) Henry, M.; Beitone, L.; Taulelle, F.; Loiseau, T.; Férey, G. *Chem. Eur. J.* **2003**, in press.

Table 4. Hyperfine Parameters from 300, 77, and 4.2 K Mössbauer Spectra of $Fe_3Al_6(PO_4)_{12}$·4*tren*·17H_2O (MIL-74) (*δ*, Isomer Shift; Γ, Half-Height Linewidth; Δ*E*, Quadrupole Splitting)

	Fe^{2+}				Fe^{3+}			
T (K)	$\delta^a \pm 0.02$ (mm/s)	$\Gamma^a \pm 0.02$ (mm/s)	$\Delta E^a \pm 0.05$ (mm/s)	$\%^b \pm 1$	$\delta^a \pm 0.02$ (mm/s)	$\Gamma^a \pm 0.02$ (mm/s)	$\Delta E^a \pm 0.05$ (mm/s)	$\% \pm 1$
			iron metal reaction **1**					
77	1.12	0.29	2.25	50				
	1.13	0.29	2.54	50				
300	1.03	0.28	2.35	50				
	1.04	0.28	2.56	50				
			iron(II) chloride reaction **2**					
4.2	1.13	0.33	2.21	48	0.35	0.26	0.55	2
	1.16	0.30	2.46	49				
77	1.11	0.33	2.21	48	0.36	0.25	0.50	4
	1.13	0.24	2.46	48				
300	1.02	0.26	2.26	48	0.27	0.26	0.50	4
	1.03	0.26	2.53	48				
			iron(III) chloride reaction **3**					
77	1.13	0.29	2.46	47	0.37	0.28	0.50	6
	1.12	0.29	2.17	47				
300	1.03	0.30	2.49	46	0.29	0.26	0.49	8
	1.02	0.30	2.27	46				

[a] Measured relative to α-Fe metal. [b] The quadrupole doublets assigned to tetrahedral Fe^{2+} sites were described by means of two components (see text).

the inorganic network. The Mössbauer local probe indicates thus a lower symmetry than that determined by the X-ray diffraction techniques. Such a statement was previously reported in the study of the MIL-74 (Zn)[28] where a certain degree of cationic Al/Zn order was observed by ^{31}P NMR but not by X-ray diffraction analysis (which indicates a rather disordered cationic network). If one considers that the central tetrahedral site (*6b*) of the enneameric unit T_5P_4 is occupied by aluminum only (see structure description section), this result rules out the possibility of describing the structure in the space group $I\bar{4}3m$. Only the site *12d* is available for the position of the T metallic atom in the $I\bar{4}3m$ configuration and a pure statistical occupancy of iron on this site would give rise to one signal. It would correspond to a full disorder situation of the T cations and this can be compared with the atomic ordering occurring in the sodalite network. Sodalite is described in different space groups depending on a disordered situation ($I\bar{4}3m$) or an ordered one ($P\bar{4}3n$). For the $P\bar{4}3n$ choice, the site *12d* is split on two equivalent crystallographic positions (*6c* and *6d*), giving rise to the occupancy of two possible sites by the iron(II) cations. It is also clear that the lack of resolution does not allow refining the relative proportions, which were varying from 52/48 to 80/14; consequently, we assumed equiprobable proportions, as listed in Table 4.

In general, iron(II) cations adopt an octahedral surrounding favored by the crystal field energy stabilization. The octahedral configuration is commonly observed in the iron(II) phosphate compounds but the occurrence of the tetrahedral one is exceptional, in contrast with the iron cations of oxidation state 3+, which may more easily adopt different types of coordination (IV, V, or VI). It is clearly established that the higher the isomer shift is, the higher is the coordination. The literature includes several works concerning the insertion of iron(III) into tetrahedral sites of the aluminophosphates of aluminosilicates open frameworks as well as the synthesis of iron(III) phosphates prepared in the presence of organic structure-directing agent. To our knowledge, only two organically templated open-framework iron phosphates have been isolated with tetrahedral iron(II) cations. They are the mixed valence Fe^{2+}/Fe^{3+} phosphate $Fe_4O(PO_4)_4$·2*en* ·H_2O and pure Fe^{2+} phosphate $FePO_4$·0.5*en*, both solids obtained with the ethylenediamine (*en*) species as template. The Mössbauer signatures of these two phases ($\delta = 1.22$ mm/s and $\Delta E = 2.84$ mm/s at 77 K,[26] and $\delta = 1.052$ mm/s and $\Delta E = 2.158$ mm/s at 300 K,[27] respectively) agree with our observations.

Depending on the iron precursor used for the hydrothermal reaction, some Mössbauer spectra show an additional doublet signal assigned to iron(III). The observed isomer shifts, which are of about 0.28 mm/s at 300 K, are in agreement with high spin Fe^{3+} cations in tetrahedral coordination. The estimated amount of Fe^{3+} in the $AlPO_4$ network is quite low: it has a maximum value of 6 ±1% for the phase obtained from iron(III) precursor (reaction **3**) and it is 2−4 ±1% for the phase obtained from iron(II) precursor (reaction **2**). However, no Fe^{3+} is observed in the phase synthesized with the iron metal precursor (reaction **1**). The Fe^{3+} content of the phase MIL-74 is also correlated to the color of the powdered product since it is colorless if the solid contains Fe^{2+} only and gets darker (from brown to black) when the amount of Fe^{3+} increases.

Magnetic Study. To check the Fe(II) valence, magnetic susceptibility measurement was performed on a sample in the temperature range from 5 to 300 K, with a SQUID magnetometer for an applied field B of 10 mT. The sample was first zero field cooled and the magnetic field was applied after stabilization of the temperature at 5 K. The dc susceptibility χ_{dc} is plotted in Figure 5a as a function of temperature. The inverse molar susceptibility curve established after correction of the sample holder signal and the core diamagnetism on MIL-74 (Fe) revealed a classical Curie−Weiss law (Figure 5b) leading to an effective moment $\mu_{eff} = 9.92$ μ_B per formula unit and to $\theta_p = 0.56$ K. Assuming a rigid coupling of the moments of the Fe^{2+}, one should

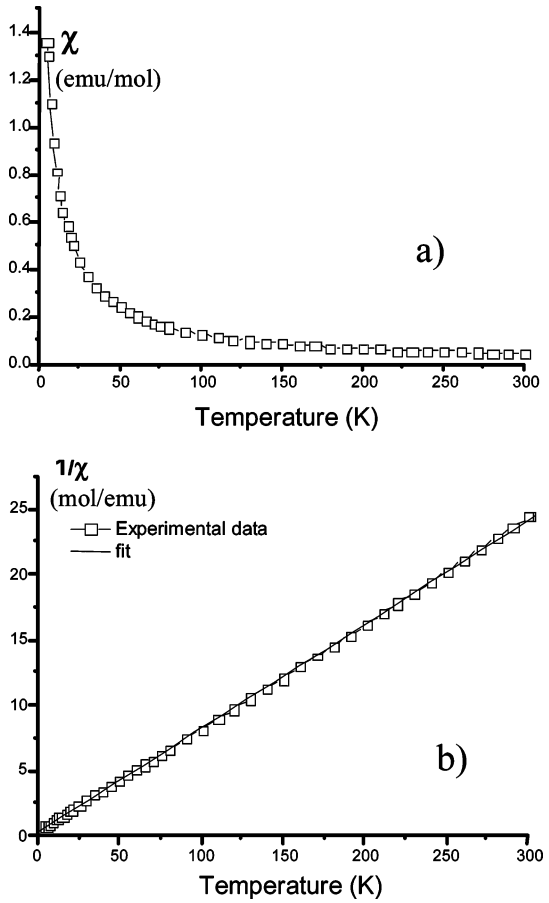

Figure 5. Susceptibility (a) and inverse magnetic susceptibility (b) of $Fe_3Al_6(PO_4)_{12}$·4*tren*·$17H_2O$ (MIL-74) as a function of temperature.

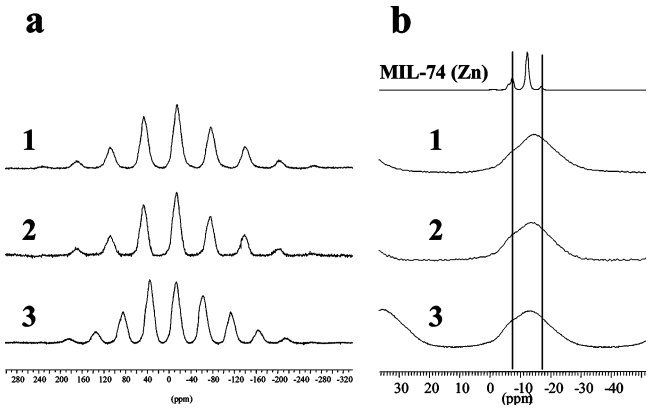

Figure 6. ^{31}P MAS NMR of MIL-74 (Zn) (12.5 kHz) and MIL-74 (Fe) from the reaction batch **1** (iron metal; 12.5 kHz), **2** (iron(II) chloride; 12.5 kHz), and **3** (iron(III) chloride; 10 kHz): (a) full spectrum; (b) expansion and position comparison with the diamagnetic phase MIL-74 (Zn).

measure 9.35 μ_B per formula unit, not far from the experimental value, in agreement with the fact that all the $Fe(II)O_4$ tetrahedra are isolated, i.e., linked through PO_4 tetrahedra.

NMR Spectroscopy. NMR spectra were recorded on three polycrystalline-powdered samples corresponding to the different starting reaction gels **1**, **2**, and **3**, as described in the synthesis section. ^{31}P spectra are shown in Figures 6 and 7. The ^{27}Al and ^{1}H NMR spectra of the sample coming from the reaction batch **1**, free of iron(III), are displayed in Figures 8 and 9, respectively.

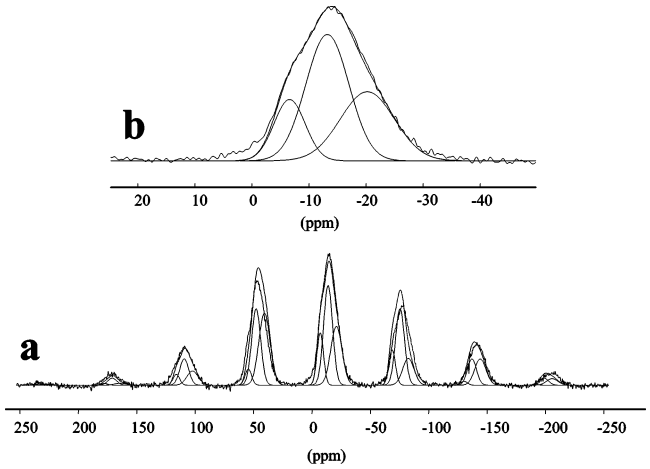

Figure 7. ^{31}P MAS NMR of MIL-74 (Fe), isotropic spinning sideband, linearly decomposed in three components, positions fixed as the diamagnetic MIL-74 (Zn) compound. The line at −21 ppm corresponds to $PAl(1_{6b})Al(2_{6c})Al(2_{6d})$, the main line at −11.5 ppm corresponds to $PAl(1_{6b})Fe(2_{6c})Al(2_{6d})$, and the line at −5 ppm corresponds to $PAl(1_{6b})Fe(2_{6c})Fe(2_{6d})$ environments: (a) full spectrum and anisotropic first-order tensor; (b) expansion of the isotropic line.

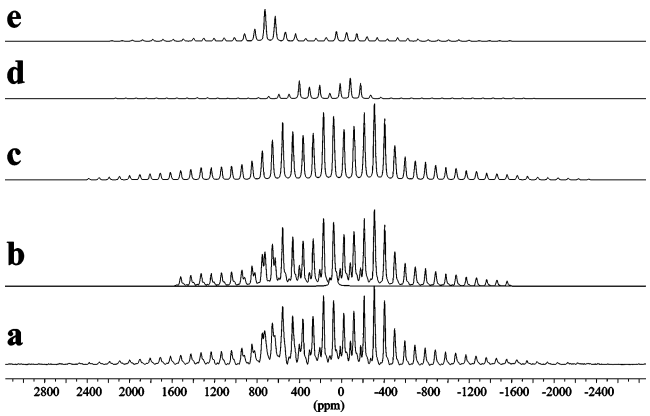

Figure 8. ^{27}Al MAS NMR of MIL-74 (Fe): (a) experimental spectrum over a 1 MHz sweep width; (b) simulation of the three components (too many sidebands to simulate all); (c) first major component with a 2350 Hz width; (d) second component with 2100 Hz; and (e) third component with 2600 Hz. The isotropic lines were difficult to locate accurately even using two MAS spinning speeds, but are in the tetrahedral region (AlO_4) between 44 and 75 ppm.

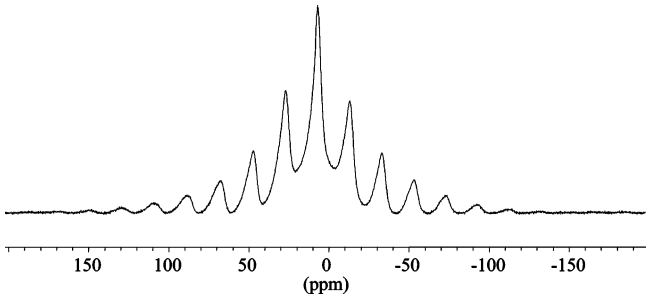

Figure 9. ^{1}H MAS NMR of MIL-74 (Fe); the loss of resolution for the inequivalent protons impedes a proper decomposition of the sub-spectra, with different anisotropic patterns.

The line widths observed for the ^{31}P spectrum are broader than the equivalent spectrum obtained for MIL-74 (Zn), with zinc, a diamagnetic cation.[28] The spectrum exhibits a pattern of spinning sidebands that spreads over 400 ppm. The ^{31}P spectrum can be decomposed as

a superimposition of three anisotropic patterns located at −21, −11.5, and −5 ppm. Each isotropic line position coincides almost with the corresponding lines observed for the MIL-74 (Zn) case and an assignment of the different components is possible by comparison with the observation of the MIL-74 (Zn) ^{31}P spectrum. The surrounding of the unique phosphorus atom (crystallographic site *24g*) differs by the nature and number of neighboring cations (Al or Fe). Accordingly, the resonance signals are attributed to the configurations $PAl(1_{6b})Al(2_{6c})Al(2_{6d})$ (−21 ppm), $PAl(1_{6b})Fe(2_{6c})Al(2_{6d})$ (−11.5 ppm), and $PAl(1_{6b})Fe(2_{6c})Fe(2_{6d})$, corresponding to the different cationic sites Al or Fe in the $P\bar{4}3n$ space group choice. No Fermi contact or pseudo-contact from the paramagnetic electrons contributes to the phosphorus shift. The presence of Fe(III) is not directly visible in the ^{31}P spectra. This is most probably due to a faster relaxation for Fe(III) than for Fe(II). The phosphorus atoms coupled to iron(III) therefore disappear. ^{31}P T_1 relaxation time is fast for Fe(II), in the range of 0.1 s, compared to that for MIL-74 (Zn) (about 60 s).

For ^{27}Al spectrum, the spinning sidebands pattern of the external transitions is also a superimposition of three sub-spectra. The decomposition of the sub-spectra is quite challenging. First, the broadening of the line widths is ranging from 2 to 2.5 kHz and degrades the resolution. Such an observation was similar for the phosphorus spectra. Second, two spinning speeds have been used to locate the isotropic shifts, but even this procedure is not as easy as usual. Some spinning speed dependent interactions may also occur. The three subspectra are consequently difficult to quantify, but one is largely dominant with about 75% of the area while the two others are in the range of 10 and 15%. The different components are observed between 44 and 75 ppm in the tetrahedral region for aluminum (AlO_4).

The ^1H spectrum does not exhibit any resolution for the three expected signals of CH_2, NH_3, and H_2O. The probe signal has been recorded for the empty probe and appears to be negligible. The spectrum displays broad spinning sidebands not totally symmetrical, as it would have been expected for a strong dipolar homonuclear coupling. The spinning sideband pattern spreads over more than 300 ppm, much broader that what would be expected for a CH_2 or H_2O dipolar coupling pattern. These observations are quite different from what is observed for the MIL-74 (Zn)[28] ^1H spectrum for which no spinning sidebands are observed between 10 and 30 kHz spinning speed. The anisotropic interaction giving rise to this spinning sidebands pattern is therefore due to the interaction between the paramagnetic electrons and hydrogen atoms.

From these observations it can be concluded that both nuclei confirm the Mössbauer observations and are consistent with the structural trends observed for MIL-74 (Zn), i.e., sites *6c* and *6d* of $P\bar{4}3n$ are occupied by Fe(II) and Al(III) with some disorder. As for MIL-74 (Zn), site occupancy of *6c* and *6d* is not a full statistical disorder, the space group cannot therefore be $I\bar{4}3m$ in principle.

The magnetic measurement showed that Fe(II) are not magnetically coupled, and the NMR isotropic shifts of phosphorus and hydrogen indicate no noticeable paramagnetic electron density. Though less clear because of the difficulty to analyze the aluminum spectra, one may assume that there, too, no paramagnetic electron density occurs on aluminum sites. The paramagnetic electrons can therefore be seen as being well localized on the iron(II) sites and are dipolar coupled to all surrounding nuclei. As there is no hyperfine contribution detected, the *g*-tensor is therefore the anisotropic interaction transported to the nuclei observed by the electron to nucleus dipolar coupling.

This is a fascinating situation for measuring all sorts of electron to nuclei coupled situations, as already proposed for paramagnetic species observed in MAS NMR.[37,38] As the disorder observed on the *6c* and *6d* sites is reproducible, all the local situations would be sensed and a full theoretical description can be expected in this case.

Conclusion

MIL-74 crystal topology is able to incorporate many cations,[39] divalent or monovalent[40] (Li or Na). Among them, several divalent paramagnetic cations have been considered. The iron case is particularly interesting because it stabilizes a tetrahedral configuration, an unusual coordination for this cation. By careful synthesis, the presence of iron(III) can be avoided and MIL-74 (Fe) behaves structurally as MIL-74 (Zn) does with some type of order/disorder on the *6c* and *6d* sites of the $P\bar{4}3n$ space group. This order/disorder is clearly observed by Mössbauer spectrometry and confirmed by ^1H, ^{31}P, and ^{27}Al MAS NMR. Iron(II) is in a high spin configuration of $S = 2$ well localized on its sites. The distances between iron sites are too large to provide a magnetic coupling between them, but they are coupled to all other neighbor nuclei. Its *g*-tensor appears therefore on all observable NMR nuclei. MIL-74 topology favors the tetrahedral coordination of iron(II). The electronic to nuclei coupling together with the MIL-74 exceptional topology may present a considerable interest in forthcoming applications.

Acknowledgment. We are grateful to Dr. M. Nogues (University Versailles) for the magnetic measurements and Dr. Mohamed Haouas (University Louis Pasteur) for his help in collecting NMR data.

Supporting Information Available: Crystallographic information file obtained from the single-crystal refinement in $I\bar{4}3m$ (cif). This material is available free of charge via the Internet at http://pubs.acs.org.

CM034535D

(37) Nayeem, A.; Yesinowski, J. P. *J. Chem. Phys.* **1988**, *89*, 4600.
(38) Lee, H.; Polenova, T.; Beer, R. H.; McDermott, A. E. *J. Am. Chem. Soc.* **1999**, *121*, 6884.
(39) Beitone, L. Ph.D. Thesis Dissertation, University of Versailles Saint-Quentin en Yvelines, January 2003.
(40) Beitone, L.; Huguenard, C.; Gansmuller, A.; Henry, M.; Taulelle, F.; Loiseau, T.; Férey, G. manuscript in preparation.